

Ultrafast photodoping and effective Fermi-Dirac distribution of the Dirac particles in Bi₂Se₃A. Crepaldi,¹ B. Ressel,² F. Cilento,² M. Zacchigna,³ C. Grazioli,^{2,*} H. Berger,¹ Ph. Bugnon,¹ K. Kern,^{1,4} M. Grioni,¹ and F. Parmigiani^{2,5,†}¹*Institute of Condensed Matter Physics (ICMP), Ecole Polytechnique Fédérale de Lausanne (EPFL), CH-1015 Lausanne, Switzerland*²*Elettra-Sincrotrone Trieste, Strada Statale 14 km 163.5, Trieste, Italy*³*CNR-IOM, Strada Statale 14 km 163.5, Trieste, Italy*⁴*Max-Planck-Institut für Festkörperforschung, D-70569 Stuttgart, Germany*⁵*Università degli Studi di Trieste, Via A. Valerio 2, Trieste, Italy*

(Received 11 September 2012; published 30 November 2012)

We exploit time- and angle-resolved photoemission spectroscopy to determine the evolution of the out-of-equilibrium electronic structure of the topological insulator Bi₂Se₃. The response of the Fermi-Dirac distribution to ultrashort IR laser pulses has been studied by modeling the dynamics of *hot* electrons after optical excitation. We disentangle a large increase in the effective temperature (T^*) from a shift of the chemical potential (μ^*), which is consequence of the ultrafast photodoping of the conduction band. The relaxation dynamics of T^* and μ^* are k independent and these two quantities uniquely define the evolution of the excited charge population. We observe that the energy dependence of the nonequilibrium charge population is solely determined by the analytical form of the effective Fermi-Dirac distribution.

DOI: [10.1103/PhysRevB.86.205133](https://doi.org/10.1103/PhysRevB.86.205133)

PACS number(s): 78.47.jd, 78.30.-j, 79.60.-i, 73.20.-r

The recent discovery of topological insulators (TIs) is renewing attention on the effects of spin-orbit interactions (SOIs) in solids, paving the road for the emergence of new quantum states of matter.¹⁻⁹ The SOI acquires particular relevance in the case of systems containing high- Z elements, leading to the lifting of the Kramers spin degeneracy in broken inversion symmetry systems, as described by Rashba and others,¹⁰⁻¹² Dresselhaus,¹³ and Rashba and Bychkov and others.^{14,15} Therefore, understanding the consequences of SOIs is of primary importance also for future technological applications in spintronics.

TIs are band insulators (semiconductors) where the conduction and the valence band states have opposite parities and their energy ordering is inverted by SOI.^{8,16} The most prominent feature of their electronic structure is the odd number of spin-polarized Dirac cones at the surface, connecting the opposite sides of the bulk band gap, resulting in topological protection from backscattering.⁷ Several classes of TIs (Bi _{x} Sb_{1- x} ,¹ Bi₂Se₃,² Bi₂Te₃,³ TlBiSe₂,^{17,18} Ternary Heusler compounds,⁴ and Pb-based TIs)^{5,19} have been discovered. Among these, Bi₂Se₃ represents a paradigmatic case, owing to the simplicity of its band structure, characterized by a single Dirac cone.^{2,9}

In TIs, the spin helicity of the metallic surface state offers the unique possibility to support spin current. Hence, spin-polarized charge distributions can be generated by circularly polarized light.^{20,21} The topological protection of the linearly dispersing surface state is expected to strongly affect the scattering mechanisms of the Dirac particle, with respect to normal metallic states. In particular, the different couplings to optical and acoustic phonon modes have been recently studied²² and the optical excitation of long-lived electron populations in the surface state might play an important role in forthcoming optospintronics devices.^{22,23}

In this paper we report on the study of the out-of-equilibrium electronic properties of Bi₂Se₃, investigated by time- and angle-resolved photoemission spectroscopy (tr-ARPES). Although conventional ARPES, with its sur-

face sensitivity, has proven to be effective and rich in information,^{1,3,6} the combined use of ultrashort laser pulses and angle-resolved photoemission experiments offers the unique possibility to explore the dynamical evolution of charge carriers after optical excitation, opening the door to the investigation of mechanisms and states hidden to experiments in the frequency domain. After optical excitation, electrons thermalize on a short time scale, owing to the fast electron-electron interaction. The resulting *hot* electron gas is described by a Fermi-Dirac (FD) distribution, with an effective electronic temperature $T^*(t)$ and an effective chemical potential $\mu^*(t)$.^{24,25} From analysis of the temporal evolution of the FD function at the Fermi wave vector k_F , we succeed in disentangling the large increase in T^* from the ultrafast shift in the chemical potential, $\Delta\mu^*$.

Our experiment reveals that the dynamics of nonequilibrium excited electron and hole populations strongly varies with the kinetic energy and the wave vector (E, k). We develop a model based on the exponential relaxation of $T^*(t)$ and $\mu^*(t)$ in the FD function to quantitatively fit the measured dynamics. We find that the relaxation times of $T^*(t)$ and $\mu^*(t)$ are k independent. The energy dependence of the charge population is then uniquely determined by the analytical form of the FD distribution. Our model, owing to the universal properties of the FD function, is more generally applicable to other tr-ARPES experiments on similar materials.

High-quality single crystals of Bi₂Se₃, in the form of platelets, were grown by the Bridgman technique. The Bi₂Se₃ samples were n-doped due to atomic vacancies and excess selenium.² tr-ARPES experiments were performed at the T-ReX Laboratory, Elettra (Trieste, Italy), with the use of a commercial Ti:Sa regenerative amplifier (Coherent RegA 9050), producing 800 nm (1.55 eV) laser pulses at a 250 kHz repetition rate, with a temporal duration of 60 fs. Samples were mounted on a He cryostat held at 100 K and cleaved *in situ* in an ultrahigh vacuum (2×10^{-10} mbar) at room temperature. The pump laser light was p polarized, and the absorbed pump

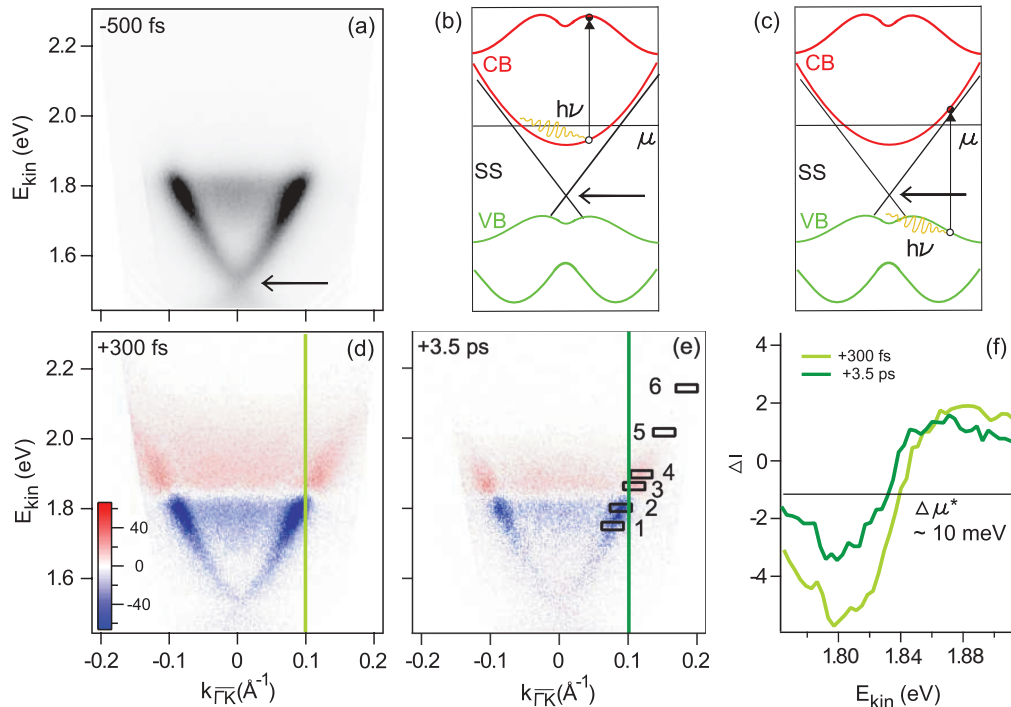


FIG. 1. (Color online) (a) ARPES band dispersion of Bi_2Se_3 at a negative delay time along the $\bar{\Gamma}\bar{K}$ high-symmetry direction. (b), (c) Schematic of interband excitation channels between conduction and conduction bands (CB-CB; b) and between valence and conduction bands (VB-CB; c). (d), (e) Pump-probe tr-ARPES signal obtained as the difference between images at positive delays (300 fs and 3.5 ps) and images at a negative delay (-500 fs). Red (blue) represents an increase (decrease) of the spectral weight. (f) Pump-probe difference energy distribution curves at the Fermi wave vector $k_F = 0.1 \text{ \AA}^{-1}$, taken from (d) and (e). The shift of the chemical potential, $\Delta\mu^*$, is experimentally resolved.

fluence was equal to $210 \mu\text{J}/\text{cm}^2$. The delay between pump and probe was introduced by modifying the optical path of the pump. Electrons were photoemitted by the s -polarized fourth harmonic at 6.2 eV , obtained by harmonic generation in phase-matched BBO crystals. Photoelectrons were analyzed and detected by a SPECS Phoibos 225 hemispherical spectrometer, with energy and angular resolution set, respectively, equal to 10 meV and 0.3° , equivalent to 0.005 \AA^{-1} . The overall temporal resolution was set to 300 fs , thus preserving the very high energy resolution required by the present experiment.

Figure 1(a) illustrates the band dispersion of Bi_2Se_3 at a negative delay time, i.e., before the arrival of the pump pulse (-500 fs), along the $\bar{\Gamma}\bar{K}$ high-symmetry direction. The energy scale reports the measured kinetic energy, since the chemical potential μ does not represent a good reference for the energy scale in the present experiment, as discussed in detail in the following. The linearly dispersing topological surface state is clearly resolved. The black arrow points towards its apex, i.e., the Dirac point. The weaker signal within the Dirac cone, at $1.7\text{--}1.84 \text{ eV}$, corresponds to the bottom of the conduction band (CB). These observations are consistent with previous ARPES results from conventional UV sources.^{2,6}

The intense pump pulses cause charge excitations between the occupied and the unoccupied parts of the CB [Fig. 1(b)], similarly to what has been observed in metals (CB-CB transitions).^{26,27} In the present case, the photon energy is higher than the band gap and this enables also interband excitations across the gap, from the fully occupied VB to the partially unoccupied CB (VB-CB transitions) [Fig. 1(c)].

Figures 1(d) and 1(e) show the pump-probe signal obtained as the difference between the ARPES images after and those before the optical perturbation. Red (blue) represents an increase (decrease) in the spectral weight. At a short delay time ($+300 \text{ fs}$) a high density of electrons populates the surface state and the CB above the chemical potential.²⁸ Such electrons result from intra- and interband transitions across the band gap. However, the temporal resolution in this experiment is not sufficient to capture the formation of the nascent nonequilibrium electron distribution, which is expected to thermalize into a hot FD distribution via electron-electron interaction, with a characteristic time shorter than 40 fs .²⁹ Figure 1(e) illustrates the reduction in the pump-probe signal at longer delay times ($+3.5 \text{ ps}$). The density of excited charge carriers is reduced, as normally observed in metals.^{26,27}

Despite this similarity, we also observe a deviation from a purely metallic response. This difference is well captured by a close inspection of the pump-probe difference energy distribution curves at the Fermi wave vector $k_F = 0.1 \text{ \AA}^{-1}$ for various delay times.²⁸ Figure 1(f) shows the two pump-probe difference energy distribution curves at $+300 \text{ fs}$ and $+3.5 \text{ ps}$. We focus our attention on the zero-crossing point, which separates the charge-depletion and the charge-accumulation regions. The zero-crossing point clearly shifts more than 10 meV . We propose that the modification of the zero-crossing energy can be explained by an ultrafast shift of the chemical potential, as recently reported in Bi_2Se_3 also by Wang *et al.*²² We interpret this effect as the consequence of the photodoping resulting from interband excitations across the gap. In the

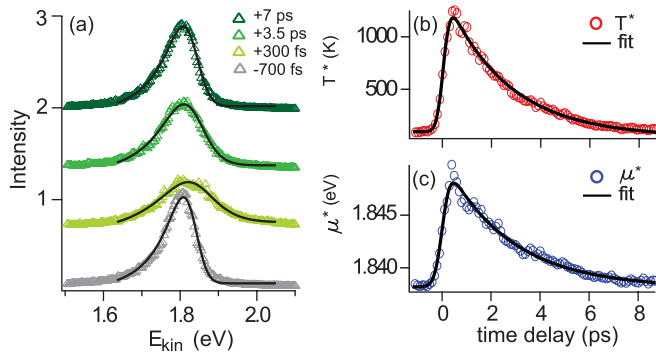


FIG. 2. (Color online) (a) Energy distribution curves at the Fermi wave vector $k_F = 0.1 \text{ \AA}^{-1}$ at four delay times (-700 fs , $+300 \text{ fs}$, $+3.5 \text{ ps}$, and $+7 \text{ ps}$). The fitting curves, in black lines, contain the FD distribution, multiplied by a Lorentzian which accounts for the surface state peak. (b) Temporal evolution of the effective temperature T^* and (c) that of the effective chemical potential μ^* , as obtained from the fit. A single decay exponential function fits the temporal dynamics well, with characteristic relaxation times equal to $\tau_T \sim 2.5 \text{ ps}$ and $\tau_\mu \sim 2.7 \text{ ps}$.

case of a nondegenerate semiconductor (i.e., μ lying in the band gap) the optically excited electrons and holes must be considered as separated systems, each with a distinct thermal distribution and with a different chemical potential, depending on the charge density.³⁰ The thermalized electron and hole distributions relax towards equilibrium via radiative processes, Auger recombination, or diffusion. A simpler relaxation via diffusion was also proposed for p-doped Bi_2Se_3 .²³ The electron-phonon scattering is unsuitable for recombining the excited electrons with holes, because the value of the gap is larger than the highest phonon energy (23 meV).^{23,31} Furthermore, for n-doped Bi_2Se_3 , the band gap acts as a bottleneck slowing down the relaxation of photoexcited holes at high binding energies (in the VB) and of low-energy holes (in the CB). This results in a transient excess of charge carriers in the CB, which is at the origin of the proposed ultrafast shift of the chemical potential.

The emergence of the ultrafast chemical shift is further supported by a quantitative analysis of the temporal evolution of the FD distribution function at k_F . Figure 2(a) displays the energy distribution curves at some selected delay times (-700 fs , $+300 \text{ fs}$, $+3.5 \text{ ps}$, and $+7 \text{ ps}$). The product of the FD distribution with a Lorentzian, describing the surface state peak, is used as a model function to fit the spectra.²⁸ The values of the effective temperature T^* and of the effective chemical potential μ^* , as obtained from the hot FD, are shown as a function of the delay time in Figs. 2(b) and 2(c), respectively. Their temporal evolution is fitted with a single decay exponential, with a proper rise time (modeled by a step function), convoluted with a Gaussian to account for the temporal resolution. The characteristic relaxation times are $\tau_T \sim 2.5 \text{ ps}$ and $\tau_\mu \sim 2.7 \text{ ps}$. The T^* relaxation is slightly slower than previously reported for p-doped Bi_2Se_3 (1.67 ps).²³ This discrepancy might be ascribed to the different doping, but it could also be related to the larger pump fluence used in the present case. The maximum value of $\Delta\mu^*$ is 12 meV , in agreement with the pump-probe difference energy distribution curve data.

The creation of a long-lived population in the CB has been proposed to be the key mechanism responsible for the slow relaxation time in the TIs Bi_2Se_3 ²³ and Bi_2Te_3 .³² In these models, the CB acts as a charge reservoir for the topological surface state at lower binding energies. Such an effect was inferred from the difference in the temporal evolution of the tr-ARPES intensity at different positions in the band structure, $I(E, k, t)$. Also in our investigation, the evolution of the surface state population at different binding energies along its linear dispersion shows a peculiar energy-dependent relaxation. However, a detailed analysis of the data suggests a different interpretation.

Figure 3 displays the $I(E, k, t)$ signal for six selected (E, k) positions below and above the chemical potential, as indicated in Fig. 1(e). We focus on the topological surface state and on the evolution of its out-of-equilibrium population. Similar trends are observed in the CB as well. We average the intensity over a narrow energy window ($<20 \text{ meV}$), and this provides us with precise information on the energy-dependent temporal evolution of the excited electrons. This constitutes an important difference from a previous study on Bi_2Te_3 , in which large energy windows were selected, enclosing distinct bands.³² The dynamics is fast for $E \gg \mu$ ($-6-$) and apparently slows down when approaching μ ($-4-$ and $-3-$). The behavior is opposite in sign but symmetric around μ ($-1-$ and $-2-$). A similar observation was reported in previous studies of p-doped Bi_2Se_3 , but the dynamics was analyzed only at a qualitative level.²³ In the following, a simple but effective model is proposed to account for this peculiar energy dependence of $I(E, k, t)$. The spectra at the various kinetic energies are fit with the model function $\zeta(E, t)$, given by the following relation:

$$\zeta(E, t) = \int_{-\infty}^{+\infty} \Theta(t' - t_0) \frac{C}{1 + \exp(E - \mu^*(t')/k_B T^*(t'))} \times G(t - t') dt' + \phi. \quad (1)$$

At time t the intensity $\zeta(E, t)$ is the result of the convolution of a Gaussian G , describing the temporal resolution, with a FD distribution. The latter is defined by the time-dependent effective temperature $T^*(t)$ and the effective chemical potential $\mu^*(t)$, which relax in time as discussed previously. Θ is a step function which accounts for the rise time. The intensity C has a weak dependence on the kinetic energy E , which we attributed to the matrix element effect. C accounts for the variation in sign in the signal between accumulation and depletion, when moving from above to below the chemical potential. Finally, ϕ represents the background. In our model the relaxation time is uniquely determined by τ_T and τ_μ , and the apparent energy dependence is conveyed by the FD distribution. The $\zeta(E, t)$ function is used to fit all the spectra (from $-1-$ to $-6-$). The results of the fit are reported as solid (black) lines in Fig. 3, showing a remarkably good agreement with the experimental data.

The microscopic description of the temporal evolution of the charge population is complex, since several de-excitation mechanisms must be considered, especially for the recombination of photocarriers across the band gap. Previous tr-ARPES studies on p-doped Bi_2Se_3 ²³ and Bi_2Te_3 ³² analyzed in detail the time evolution of the tr-ARPES intensity $I(E, k, t)$. In those studies a delay between the dynamics of the surface state and the CB charge carriers was revealed. This delay was interpreted

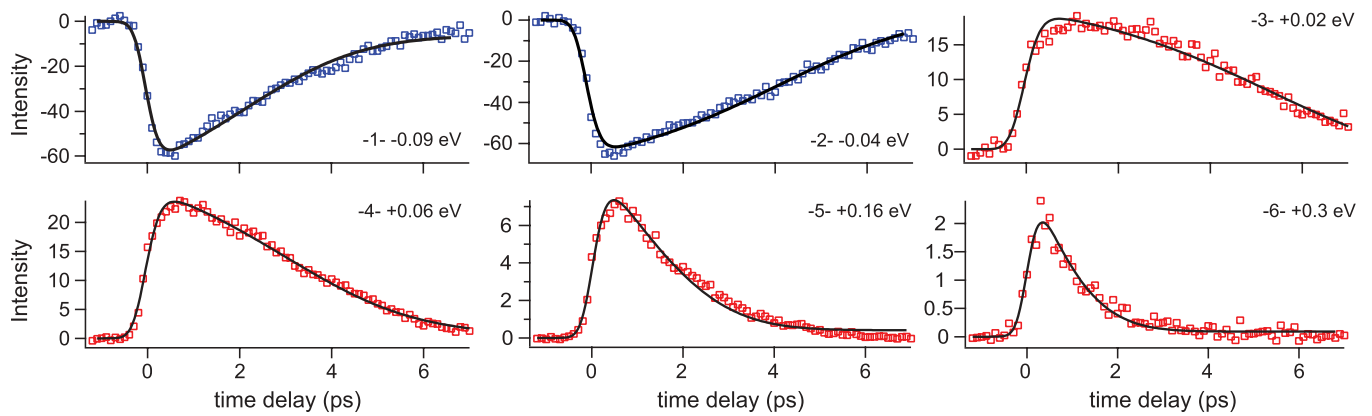


FIG. 3. (Color online) Ultrafast evolution of the nonequilibrium charge population in the topological surface state at six energies, along its linear dispersion, as indicated in Fig. 1(e). The results of the fitting routine are displayed as solid (black) lines. The model function results from the intensity of the Fermi-Dirac distribution at that energy at an effective temperature T^* and with an effective chemical potential μ^* , which relax exponentially in time as shown, respectively, in Figs. 2(b) and 2(c).

as the result of a multistep relaxation process of the electrons excited in upper branches of the CB. Therefore, the CB was proposed to act as a charge reservoir for a long-lived electron population in the Dirac cone. The Fig. 3 data analysis proves that the long-lasting electronic dynamics in the photodoped Bi_2Se_3 surface state is governed by the evolution of the FD distribution. Recently, also Wang *et al.* focused their attention on the time evolution of the out-of-equilibrium FD distribution in Bi_2Se_3 .²² The authors, by studying as a function of the temperature the response of Bi_2Se_3 with varied stoichiometries, were able to disentangle the role played by optical and acoustic phonons in the scattering mechanisms between the CB and the surface state. From the evolution of T^* and μ^* they pointed out that at low temperatures the coupling between the bulk and the surface state is suppressed. However, in the present experiment, because of the temperature (100 K), it was not possible to separate acoustic and optical phonon cooling. Nevertheless, the scope of our work is to interpret the temporal evolution of the tr-ARPES intensity $I(E, k, t)$. This is properly modeled by a time-dependent effective FD function, uniquely determined by the effective electronic temperature T^* and the effective chemical potential μ^* . Moreover, our findings indicate that this pump fluence, and the consequent large increase in the effective electronic temperature, might hinder the formation of light-induced spin currents at the Dirac cone. This suggests that the low-fluence regime must be investigated in detail in order to reveal some of the nontrivial aspects of the carrier dynamics.

In summary, we have investigated in detail the time-dependent electronic thermal distribution after optical excitation in Bi_2Se_3 . We find that, at all delay times, electrons in the surface states are thermalized. Their distribution can be

approximated by an effective FD function whose temperature T^* and chemical potential μ^* relax in time with a decaying exponential behavior. The fast electronic thermalization, below the experimental resolution (300 fs), is ensured by the characteristic time of the electron-electron interaction (<40 fs).²⁹ The variation in the effective chemical potential is interpreted as the result of the ultrafast photodoping of the CB, similarly to what was recently reported by Wang *et al.*²² The relaxation time of T^* and μ^* are, respectively, equal to $\tau_T \sim 2.5$ ps and $\tau_\mu \sim 2.7$ ps. The former is compatible with a mechanism of energy relaxation to the lattice mediated by the electron-phonon interaction. The latter is related to the relaxation of the excess charge in the CB via diffusion.

We propose a model which relies only on the inherent properties of the FD distribution function and, therefore, provides a viable interpretation for the similar energy dependence of the electronic dynamics in a different material³² and in p-doped Bi_2Se_3 .²³ The effect of topological protection during the relaxation of the Dirac cone charge population may provide the clue for designing new optospintronic devices.²⁰ Our model paves the way for future investigations of the response of topologically protected versus conventional semiconductors.

We thank C. Tournier-Colletta for clarifying discussions. This work was supported in part by the Italian Ministry of University and Research under Grant Nos. FIRB-RBAP045JF2 and FIRB-RBAP06AWK3 and by the European Community–Research Infrastructure Action under the FP6 “Structuring the European Research Area” program through the Integrated Infrastructure Initiative “Integrating Activity on Synchrotron and Free Electron Laser Science,” Contract No. RII3-CT-2004-506008.

*Present address: University of Nova Gorica, Vipavska 11 c, 5270 Ajdovscina, Slovenia.

†Corresponding author: fulvio.parmigiani@elettra.trieste.it

¹D. Hsieh, D. Qian, L. Wray, Y. Xia, Y. S. Hor, R. J. Cava, and M. Z. Hasan, *Nature* **452**, 970 (2008).

²Y. Xia, D. Qian, D. Hsieh, L. Wray, A. Pal, H. Lin, A. Bansil, D. Grauer, Y. S. Hor, R. J. Cava *et al.*, *Nat. Phys.* **5**, 398 (2009).

³Y. L. Chen, J. G. Analytis, J.-H. Chu, Z. K. Liu, S.-K. Mo, X. L. Qi, H. J. Zhang, D. H. Lu, X. Dai, Z. Fang *et al.*, *Science* **325**, 178 (2009).

- ⁴S. Chadov, X. Qi, J. Kübler, G. H. Fecher, C. Felser, and S. C. Zhang, *Nat. Mat.* **9**, 541 (2010).
- ⁵S. V. Eremeev, G. Landolt, T. V. Menshchikova, B. Slomski, Y. M. Koroteev, Z. S. Aliev, M. B. Babanly, J. Henk, A. Ernst, L. Patthey *et al.*, *Nat. Commun.* **3**, 1 (2012).
- ⁶M. Bianchi, D. Guan, S. Bao, J. Mi, B. B. Iversen, P. D. King, and P. Hofmann, *Nat. Commun.* **1**, 1 (2010).
- ⁷P. Roushan, J. Seo, C. V. Parker, Y. S. Hor, D. Hsieh, D. Qian, A. Richardella, M. Z. Hasan, R. J. Cava, and A. Yazdani, *Nature* **460**, 1106 (2009).
- ⁸L. Fu, C. L. Kane, and E. J. Mele, *Phys. Rev. Lett.* **98**, 106803 (2007).
- ⁹H. Zhang, C.-X. Liu, X.-L. Qi, X. Dai, Z. Fang, and S.-C. Zhang, *Nat. Phys.* **5**, 438 (2009).
- ¹⁰E. Rashba, *Sov. Phys. Solid State* **2**, 1109 (1960).
- ¹¹K. Ishizaka, M. S. Bahramy, H. Murakawa, M. Sakano, T. Shimojima, T. Sonobe, K. Koizumi, S. Shin, H. Miyahara, A. Kimura *et al.*, *Nat. Mat.* **10**, 521 (2011).
- ¹²A. Crepaldi, L. Moreschini, G. Autés, C. Tournier-Colletta, S. Moser, N. Virk, H. Berger, P. Bugnon, Y. J. Chang, K. Kern, A. Bostwick, E. Rotenberg, O. V. Yazyev, and M. Grioni, *Phys. Rev. Lett.* **109**, 096903 (2012).
- ¹³G. Dresselhaus, *Phys. Rev.* **100**, 580 (1955).
- ¹⁴Y. A. Bychkov and E. I. Rashba, *JETP Lett.* **39**, 278 (1984).
- ¹⁵S. LaShell, B. A. McDougall, and E. Jensen, *Phys. Rev. Lett.* **77**, 3419 (1996).
- ¹⁶L. Fu and C. L. Kane, *Phys. Rev. B* **76**, 045302 (2007).
- ¹⁷Y. L. Chen, Z. K. Liu, J. G. Analytis, J.-H. Chu, H. J. Zhang, B. H. Yan, S.-K. Mo, R. G. Moore, D. H. Lu, I. R. Fisher *et al.*, *Phys. Rev. Lett.* **105**, 266401 (2010).
- ¹⁸K. Kuroda, M. Ye, A. Kimura, S. Eremeev, E. E. Krasovskii, E. Chulkov, Y. Ueda, K. Miyamoto, T. Okuda, K. Shimada *et al.*, *Phys. Rev. Lett.* **105**, 146801 (2010).
- ¹⁹S.-Y. Xu, A. Wray, Y. Xia, R. Shankar, A. Petersen, A. Fedorov, H. Lin, A. Bansil, Y. S. Hor, D. Grauer *et al.*, [arXiv:1007.5111](https://arxiv.org/abs/1007.5111).
- ²⁰J. W. McIver, D. Hsieh, H. Steinberg, P. Jarillo-Herrero, and N. Gedik, *Nat. Nanotech.* **7**, 96 (2012).
- ²¹D. Hsieh, F. Mahmood, J. W. McIver, D. R. Gardner, Y. S. Lee, and N. Gedik, *Phys. Rev. Lett.* **107**, 077401 (2011).
- ²²Y. H. Wang, D. Hsieh, E. J. Sie, H. Steinberg, D. R. Gardner, Y. S. Lee, P. Jarillo-Herrero, and N. Gedik, *Phys. Rev. Lett.* **109**, 127401 (2012).
- ²³J. A. Sobota, S. Yang, J. G. Analytis, Y. L. Chen, I. R. Fisher, P. S. Kirchmann, and Z.-X. Shen, *Phys. Rev. Lett.* **108**, 117403 (2012).
- ²⁴P. B. Allen, *Phys. Rev. Lett.* **59**, 1460 (1987).
- ²⁵L. Perfetti, P. A. Loukakos, M. Lisowski, U. Bovensiepen, H. Eisaki, and M. Wolf, *Phys. Rev. Lett.* **99**, 197001 (2007).
- ²⁶W. S. Fann, R. Storz, H. W. K. Tom, and J. Bokor, *Phys. Rev. B* **46**, 13592 (1992).
- ²⁷M. Lisowski, P. Loukakos, U. Bovensiepen, J. Stähler, C. Gahl, and M. Wolf, *Appl. Phys. A* **78**, 165176 (2004).
- ²⁸See Supplemental Material at <http://link.aps.org/supplemental/10.1103/PhysRevB.86.205133> for videos of the dynamics of the pump-probe tr-ARPES and differential energy distribution curves and for a detailed description of the energy distribution curve data analysis.
- ²⁹S. R. Park, W. S. Jung, C. Kim, D. J. Song, C. Kim, S. Kimura, K. D. Lee, and N. Hur, *Phys. Rev. B* **81**, 041405 (2010).
- ³⁰A. Othonos, *J. Appl. Phys.* **83**, 1789 (1998).
- ³¹W. Richter and C. R. Becker, *Phys. Status Solidi B* **84**, 619 (1977).
- ³²M. Hajlaoui, E. Papalazarou, J. Mauchain, G. Lantz, N. Moisan, D. Boschetto, Z. Jiang, I. Miotkowski, Y. P. Chen, A. Taleb-Ibrahimi *et al.*, *Nano Lett.* **12**, 3532 (2012).